ELSEVIER

International Journal of Inorganic Materials 3 (2001) 401–407

International Journal of Inorganic Materials

Solid-state synthesis and characterization of $LiNi_yCo_{1-y}O_2$ ($0.0 \leq y \leq 0.4$)

B. Ramesh Babu, P. Periasamy, R. Thirunakaran, N. Kalaiselvi, T. Prem Kumar, N.G. Renganathan, M. Raghavan, N. Muniyandi*

Lithium Batteries Division, Central Electrochemical Research Institute, Karaikudi 630 006, Tamil Nadu, India

Received 20 April 2000; accepted 13 February 2001

Abstract

Quaternary oxides of compositions $LiNi_yCo_{1-y}O_2$ (y=0.0, 0.1, 0.2, 0.3 and 0.4) were synthesized using a solid-state route from carbonate precursors. Material characterization was carried out using XRD, FTIR and particle size analyses. The formation patterns of the products are discussed from TG-DTA results. Nickel-rich compositions gave higher discharge capacities and smaller hysteresis in the charge–discharge cycling profiles which make them more attractive candidates than the unsubstituted $LiCoO_2$ for use in high energy lithium-ion cells. However, the lower loss in capacity per cycle for cells with $LiCoO_2$, as determined from charge–discharge studies up to 25 cycles, makes them more suitable than the substituted oxides for long cycle-life cells with low fade. © 2001 Published by Elsevier Science Ltd.

Keywords: A. Layered oxides; B. Intercalation compounds; B. Solid-state synthesis; C. Electrochemical properties; D. Energy storage

1. Introduction

Lithium rocking chair cells represent the state-of-the-art in portable power sources for a variety of consumer and communications gadgets. Such cells employ a lithium-laden 3d transition metal ternary oxide cathode ($LiCoO_2$, $LiNiO_2$ or $LiMn_2O_4$) in conjunction with a graphite or coke anode. A critical component that determines the performance of these cells is the lithium-intercalating cathode material. Since the commercialization of the carbon/lithium cobalt oxide cell by Sony Energytec in 1990, solid solutions of the α-$NaFeO_2$ type $LiNi_yCo_{1-y}O_2$ [1–4] and their endmembers $LiCoO_2$ and $LiNiO_2$ have received much attention. The two homologous endmembers possess high theoretical discharge capacities of 274 mAh/g which, however, cannot be tapped fully owing to structural instabilities in the former and cation disorder in the latter. Mizushima et al. [5] have reported that the CoO_2 sublattice in $LiCoO_2$ remains unaffected for the range $0.33 \leq x \leq 1.00$ in Li_xCoO_2. However, for $x < 0.33$, based on their observation of fewer and weaker X-ray diffraction (XRD) peaks, the authors [5] suggest a reduction in crystallinity and possible destabilization of the Li_xCoO_2 material. In the case of Li_xNiO_2, Dahn et al. [6], based on their in situ XRD measurements, showed that only one phase was present in the system for the range $0.4 \leq x \leq 1.00$; however, at low x values they observed that insertion and deinsertion of lithium into the lattice resulted in a conspicuous hysteresis in the a axis and volume of the unit cell which they attributed to the migration of nickel ions into the lithium sites.

$LiNi_yCo_{1-y}O_2$ solid solutions show lower insertion potentials compared to the pure $LiCoO_2$ phase. Nickel-substituted $LiCoO_2$ phases are, therefore, expected to be oxidatively less taxing on the electrolyte and possibly to retain good lamellar structure upon repeated cycling [2–4,7–9]. In this paper we compare the physicochemical characteristics and electrochemical charge–discharge be-

*Corresponding author. Tel.: +91-45-652-7552; fax: +91-45-652-7779.

E-mail address: battery@cscecri.ren.nic.in (N. Muniyandi).

1466-6049/01/$ – see front matter
PII: S1466-6049(01)00023-X

haviour of $LiCoO_2$ and $LiNi_yCo_{1-y}O_2$ (y=0.1, 0.2, 0.3 and 0.4) obtained by solid-state fusion synthesis from carbonate precursors.

2. Experimental

2.1. Cathode preparation

Li_2CO_3 (99.9%, Merck, India), $NiCO_3 \cdot 6H_2O$ (Aldrich, USA) and $CoCO_3$ (Acros Organics, Belgium) were taken in the appropriate stoichiometric amounts and thoroughly mixed in hexane using a mortar and a pestle. The mixtures were initially heated at 400°C for 6 h followed by firing at 800 and 900°C in air for 18 h at each temperature with intermittent grinding for 4 h. The extended grinding was resorted to in order to avoid compositional non-homogeneity in the final product. The grinding would greatly reduce diffusion barriers that lace grains of the product in the form of undesirable phases or impurities. The reaction products were ground and stored in a desiccator with fused calcium chloride as the desiccant. For preparation of the electrodes, the required oxide powder was well mixed with 5% polyvinylidene fluoride and 10% acetylene black in *N*-methylpyrrolidone to a slurry. The slurry was then brush-coated on an aluminum foil substrate and dried in a vacuum oven maintained at 150°C for 6 h. The weight of the cathode active material thus loaded on a 2-cm diameter disc was 0.056 g. Cathode-limited cells were assembled in an argon-filled MBraun glove box using standard 2016 coin cell hardware with lithium as the anode, 1 M $LiAsF_6$ in 1:1 EC/DEC as the electrolyte and Celgard 2400 separator.

2.2. Material characterization

Powder X-ray diffractograms were recorded on a Jeol JDX 8030 X-ray diffractometer (Japan) with a nickel-filtered CuKα radiation. Lattice parameters were refined against an internal standard of silicon. FTIR spectra of the samples were obtained by the KBr pellet method using a Perkin-Elmer FTIR Spectrometer-Paragon 500 model, UK. For thermal analysis, the STA 1500 simultaneous thermal analysis system of Polymer Laboratories (UK) was employed.

3. Results and discussion

3.1. X-ray diffraction studies

Characteristic powder XRD profiles of $LiCoO_2$ and the nickel-substituted $LiCoO_2$ are shown in Fig. 1a–e. The profiles show only slight changes as the stoichiometry of nickel in the compounds is varied. Since Ni^{3+} substitutes isomorphically for Co^{3+} in the solid solutions considered

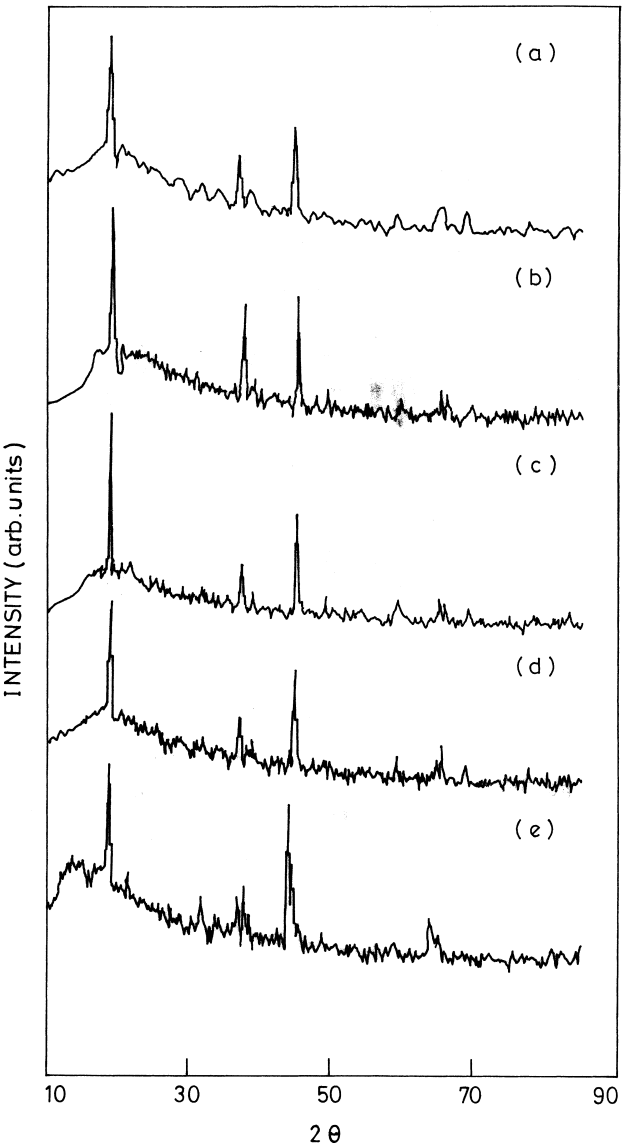

Fig. 1. Powder X-ray diffraction profiles of (a) $LiCoO_2$ and $LiNi_yCo_{1-y}O_2$: (b) y=0.1; (c) y=0.2; (d) y=0.3; and (e) y=0.4.

here, the lithium ions should occupy octahedral sites between [$Ni_yCo_{1-y}O_2$] infinite slabs formed by edge-sharing [$Ni_yCo_{1-y}O_6$] octahedra. Therefore, all the XRD patterns for $LiCoO_2$ and the solid solutions were indexed in the hexagonal system assuming the *R3m* symmetry [5,10]. However, in the case of the nickel-substituted phases one must look for existence of nickel ions in the lithium layers because of the propensity of this ion to mix with the lithium layer as often obtains in $LiNiO_2$. The ratio of the intensities of the XRD lines $I_{(003)}/I_{(104)}$ and/or $I_{(101)}/I_{(102,006)}$ are considered to be indicators of ordering of lithium and transition metal ions (Ni and/or Co) [6,11]. This cation mixing disorder can be detrimental to the electrochemical performance of the cathode material manifesting as diminished rechargeable capacity and poor lithium intercalation properties. The integrated ratios of the

intensity of the (003) peak to that of the (104) peak in our case are 1.33 for the pristine $LiCoO_2$, and 1.20, 1.51, 1.56 and 1.45 for samples with $y=0.1$, 0.2, 0.3 and 0.4, respectively. This compares favourably with the value of 1.13 reported by Fujita et al. [12] for $LiNi_{0.85}Co_{0.15}O_2$ prepared in air. However, the same authors report values of 1.49 and 1.57 for $LiNiO_2$ and $LiNi_{0.85}Co_{0.15}O_2$, respectively, both prepared in flowing oxygen [12]. At a value of <1.2 for this ratio, the (108) and (110) peaks or the (006) and (102) peaks become hardly distinguishable; the cation mixing can adversely affect electrochemical performance [13]. The presence of Ni^{3+} in the Li^+ sites is also believed to impede diffusion of lithium ions in the host lattice.

The ratio of lattice parameters a and c (c/a) is characteristic of the anisotropy of the structure. The variation of the c/a ratio as a function of the nickel content in $LiNi_yCo_{1-y}O_2$ is presented in Table 1; values of c/a fall between 4.982 and 4.966. Thus the substitution of nickel for cobalt in $LiCoO_2$ tends to metamorphose the electrochemically active hexagonal close packed *R3m* symmetry (for which the c/a value is 4.99) into an electrochemically inactive cubic close packed *Fm3m* crystal structure (for which the c/a ratio is 4.90) [14]. However, the fact that the c/a value does not fall below 4.96 is indicative of the fact that no cation mixing occurs up to a value of $y=0.4$ in $LiNi_yCo_{1-y}O_2$ [15]. This is in agreement with the results of Julien et al. [16] which indicated no cation mixing between the nickel and lithium in the octahedral sites up to a value of $y=0.5$ in $LiNi_yCo_{1-y}O_2$ prepared by sol–gel and combustion methods.

3.2. FTIR studies

FTIR data help in understanding local environmental effects of cations in a lattice [17,18]. Fig. 2a–e depicts changes in FTIR spectra as the nickel content in $LiNi_yCo_{1-y}O_2$ is increased. The evolution of the spectra is similar to that reported by Ohzuku et al. [4]. Not all the absorption peaks are assigned here; however, based on the FTIR data reported by Julien et al. [16], we can assign the peaks in the 510–520 cm^{-1} and 580–610 cm^{-1} regions to the asymmetric stretching modes of $\{MO_6\}$ octahedra (M= Ni or Co). Further, the shift of the absorption peaks in the 500–700 cm^{-1} region towards lower wavenumbers as the nickel content increases is in agreement with the observations of Ohzuku et al. [4]. This shift is attributed to an increase in the average transition metal–oxygen bond in the $[MO_6]$ octahedra as more and more cobalt ions are substituted with nickel [4]. Furthermore, the broadening of the peaks in the 500–700 cm^{-1} region with an increase in y may be ascribed to non-uniform distribution of the transition metal cations which seems to correlate well with the decreasing value of the c/a ratio as determined from our XRD studies.

Table 1
Lattice parameters of $LiNi_yCo_{1-y}O_2$ ($0\leq y\leq 0.4$) from XRD data

Composition	c (Å)	a (Å)	c/a
$LiCoO_2$	14.048	2.820	4.982
$LiNi_{0.1}Co_{0.9}O_2$	14.068	2.827	4.975
$LiNi_{0.2}Co_{0.8}O_2$	14.098	2.835	4.973
$LiNi_{0.3}Co_{0.7}O_2$	14.118	2.840	4.971
$LiNi_{0.4}Co_{0.6}O_2$	14.133	2.846	4.966

3.3. Thermal analytical studies

The TG/DTA curves obtained with precursors in stoichiometric amounts corresponding to $y=0$, 0.1, 0.2, 0.3 and 0.4 in $LiNi_yCo_{1-y}O_2$ are presented in Figs. 3–7. The thermal profiles for the formation of the products from the carbonate precursors may be divided into two regions: a low-temperature region (up to 300°C) followed by a high-temperature region (up to 800°C). The pattern seems to change little as the nickel content in the product is increased. In fact, the TG/DTA curves for the formation of the nickel-substituted compounds show a striking similarity to that of the parent compound, $LiCoO_2$. The low-temperature region shows an exothermic peak between 250 and 300°C corresponding to a reaction that Li_2CO_3 and $CoCO_3$ enter into in air [19]. Studies of the decomposition patterns of $CoCO_3$ and Li_2CO_3 in air have shown that $CoCO_3$ undergoes an endothermic reaction to yield Co_3O_4 around 270–280°C [19,20] and that Li_2CO_3 is stable in air up to ~750°C and melts at 723°C [21]. The observed exothermic peak is thus due to a possible reaction between the finely divided Co_3O_4 and Li_2CO_3 to form Co_3O_4 with interstitial Li_2O [19]. The results are not surprising given the fact that several carbonates upon mixing produce easily decomposable mixtures [22].

The reactions in the low-temperature region may thus be written as

$$6CoCO_3 + O_2 \rightarrow 2\,Co_3O_4 + 6\,CO_2$$

followed by the partial decomposition of Li_2CO_3 in the presence of Co_3O_4

$$Li_2CO_3 + Co_3O_4 \rightarrow Li_2O - Co_3O_4 + CO_2$$

The presence of CO_2 in the reaction zone is believed to trigger the melting of an eutectic of composition Li_2CO_3–Li_2O–LiOH around 410°C [23,24]. Meanwhile, in the nickel-containing samples, $NiCO_3\cdot 6H_2O$ decomposes at 140°C to the basic carbonate which immediately loses CO_2 and H_2O to produce NiO [25]

$$NiCO_3\cdot 6H_2O \rightarrow a NiCO_3\cdot b Ni(OH)_2\cdot c H_2O \rightarrow NiO$$

where $a=2$, $b=3$ and $c=4$.

The high-temperature region is supposed to support the reaction between Li_2CO_3 and the low-temperature reaction product according to the equation

$$4Li_2O - Co_3O_4 + 2\,Li_2CO_3 + O_2 \rightarrow 12\,LiCoO_2 + 2\,CO_2$$

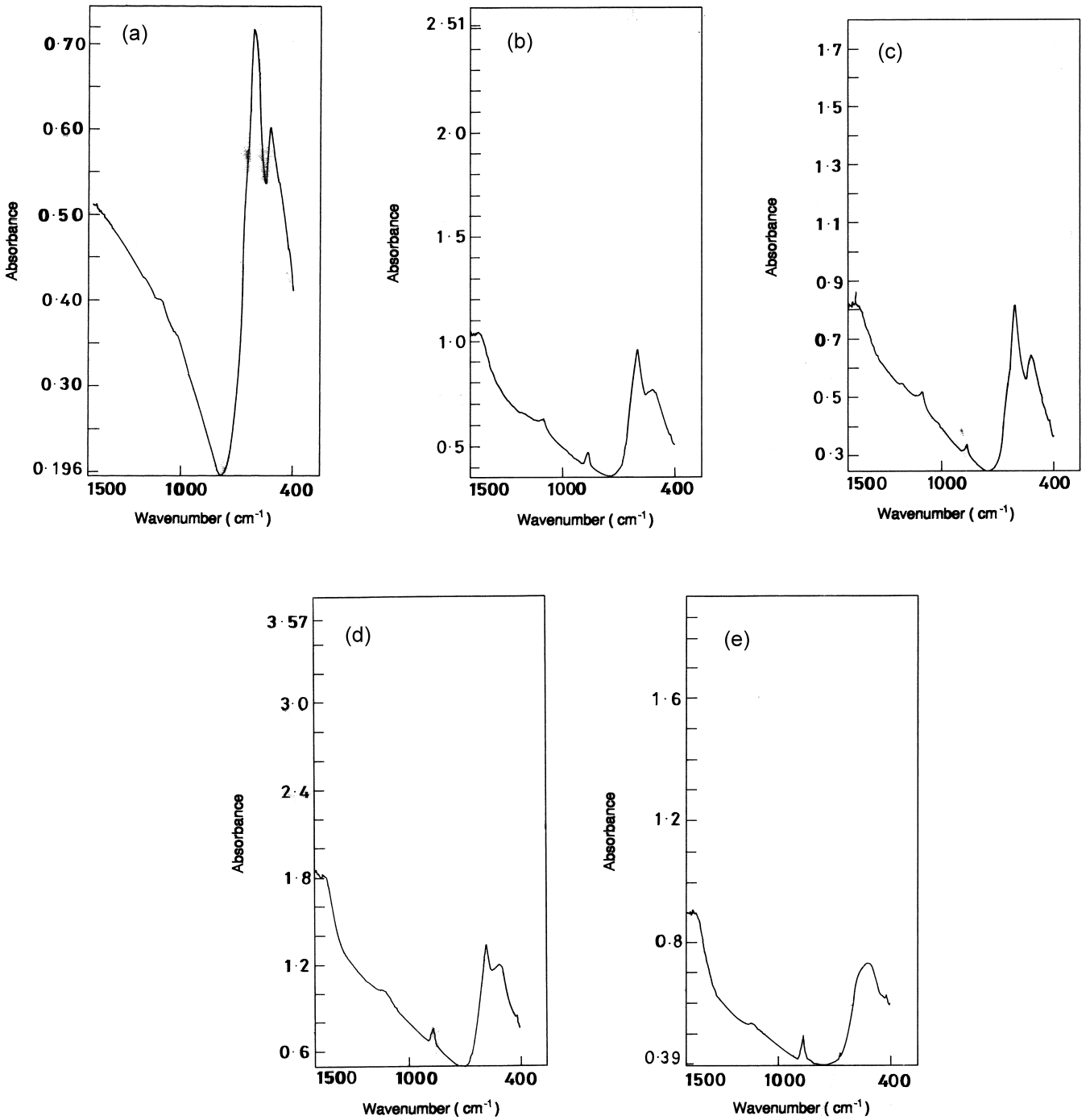

Fig. 2. FTIR spectra of $LiNi_yCo_{1-y}O_2$ as a function of nickel content. (a) $y=0.0$; (b) $y=0.1$; (c) $y=0.2$; (d) $y=0.3$; and (e) $y=0.4$.

or

$$4\,Co_3O_4 + 6\,Li_2CO_3 + O_2 \rightarrow 12\,LiCoO_2 + 6\,CO_2$$

The reaction may also proceed via a reaction of Co_3O_4 with Li_2O, although $LiCoO_2$ has been demonstrated to have been formed at temperatures as low as 400°C [26–30]. Additionally, in nickel-laden samples NiO reacts with Li_2CO_3 in air to produce $LiNiO_2$.

3.4. Charge–discharge studies

Fig. 8 shows the first charging curves of Li–$LiNi_yCo_{1-y}O_2$ cells up to a stage corresponding to the deinsertion of 0.6 Li. The profiles closely resemble those reported in the literature [4,6,9,14,16,31]. A decreasing trend in the operating voltage of the cell may be noted as the y value is increased. This is only to be expected since the Ni^{4+}–Ni^{3+} has a lower potential vs. Li^+–Li compared

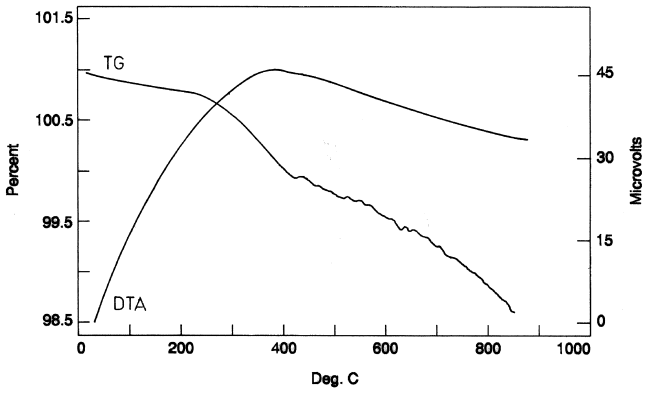

Fig. 3. TG/DTA curves of precursors for $LiCoO_{2.}$.

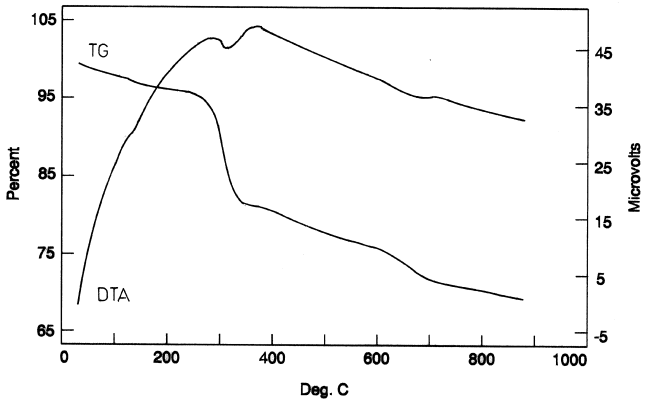

Fig. 4. TG/DTA curves of precursors for $LiNi_{0.1}Co_{0.9}O_2$.

to that for the Co^{4+}–Co^{3+} couple. Moreover, for all the nickel-laden cathodes there appears a perceptible change in the slope of the voltage profiles in the 3.5–3.8 V region, the slope change becoming more pronounced as the nickel content increases. Further, the domain of slope change shifts nearly in accordance with the fraction of cobalt substituted with nickel. Thus one may expect the oxidation of Ni^{3+} to precede that of Co^{3+} in $LiNi_yCo_{1-y}O_2$. The preferential oxidation of Ni^{3+} in $LiNi_yCo_{1-y}O_2$ upon

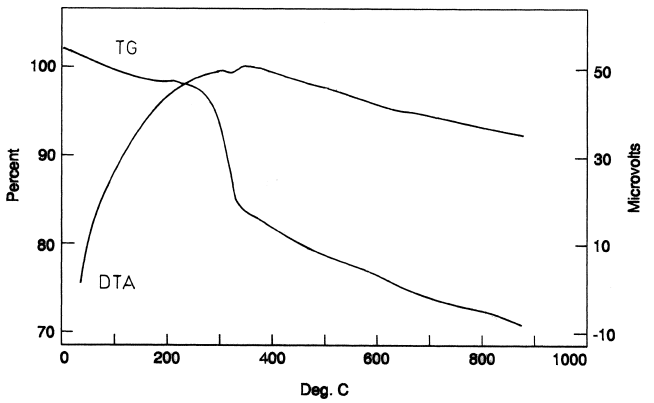

Fig. 5. TG/DTA curves of precursors for $LiNi_{0.2}Co_{0.8}O_{2.}$.

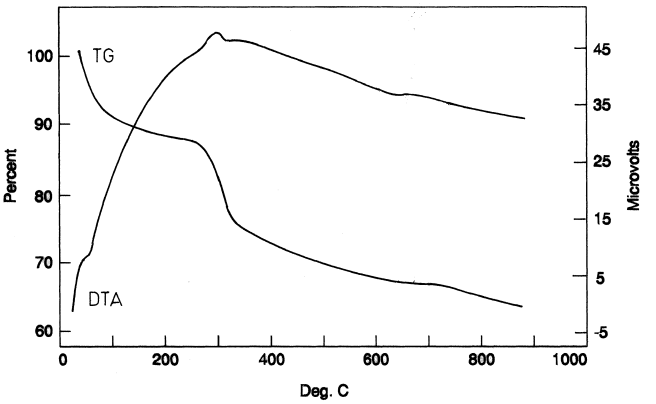

Fig. 6. TG/DTA curves of precursors for $LiNi_{0.3}Co_{0.7}O_{2.}$.

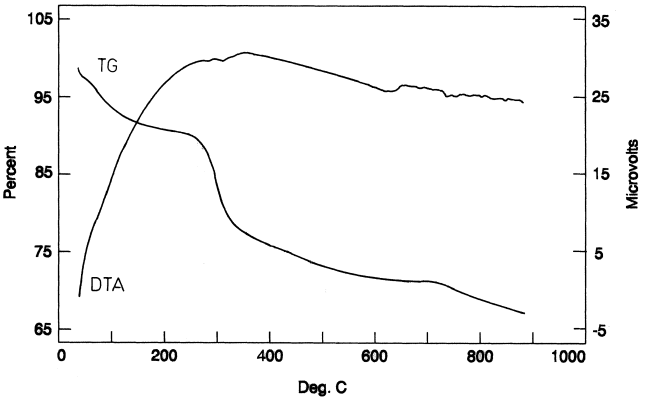

Fig. 7. TG/DTA curves of precursors for $LiNi_{0.4}Co_{0.6}O_{2.}$.

electrochemical deintercalation has been demonstrated by Saadoune and Delmas [9] and by Alcantara et al. [32] in their studies on the acid delithiation of $LiCo_yNi_{1-y}O_2$ solid solutions. The lithium intercalation–deintercalation

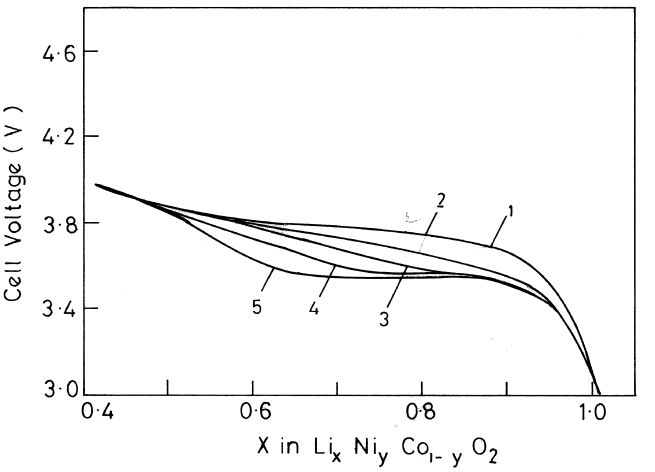

Fig. 8. First charging curves of Li–$LiNi_yCo_{1-y}O_2$ cells. (1) $y=0.0$; (2) $y=0.1$; (3) $y=0.2$; (4) $y=0.3$; and (5) $y=0.4$. Charging current: 50 μA.

reaction in the system under consideration may thus be written as a two-step process

$$Li[Ni_y^{3+}Co_{1-y}^{3+}]O_2 \Leftrightarrow$$

$$\square_y Li_{1-y}[Ni_y^{4+}Co_{1-y}^{3+}]O_2 + yLi^+ + ye^- \Leftrightarrow$$

$$\square_x Li_{1-x}[Ni_y^{4+}Co_{x-y}^{4+}Co_{1-x}^{3+}]O_2 + (x-y)Li^+ + (x-y)e^-$$

Several workers have observed a two-step lithium extraction process between 3.6 and 4.0 V in $LiCoO_2$ which has been attributed to the removal of lithium from 3*a* octahedral sites followed by the removal of further lithium and formation of a second phase with lithium ions in both tetrahedral and octahedral sites. No evidence of such a two-step lithium deintercalation process, which may be expected to occur in cobalt-rich phases as well, could be seen in our charge–discharge curves. Fig. 9 presents the charge–discharge curves of $LiCoO_2$ and $LiNi_yCo_{1-y}O_2$ in the 1st and 25th cycles at a charge–discharge rate of 50 μA. For $LiCoO_2$ the specific charging and discharging capacities in the 1st cycle were 146 and 132 mAh, respectively, between 4.2 and 3.0 V cut-offs. The corresponding values for $LiNi_{0.4}Co_{0.6}O_2$ were 160 and 148 mAh. In the 25th cycle, the values dropped to 126 and 118 mAh for $LiCoO_2$ and to 134 and 125 for $LiNi_{0.4}Co_{0.6}O_2$. The average discharge voltages recorded for $LiCoO_2$ and $LiNi_{0.4}Co_{0.6}O_2$ were 3.85 and 3.63 V, respectively. In fact, all the nickel-laden cathode materials gave higher discharge capacities at lower operating voltages than $LiCoO_2$. Further, the nickel-containing cathodes exhibited reduced hysteresis in their charge–discharge profiles and hence could be more suitable materials than $LiCoO_2$ in high-voltage lithium/lithium-ion cells.

Fig. 10 depicts the reduced hysteresis in the charge–discharge profile of $LiNi_{0.4}Co_{0.6}O_2$ as compared to that in $LiCoO_2$. In fact, it has been observed that this hysteresis becomes less pronounced as the amount of nickel in the solid solution increases. The reduced hysteresis in the nickel-rich compounds makes them better candidates for use in high-voltage cells.

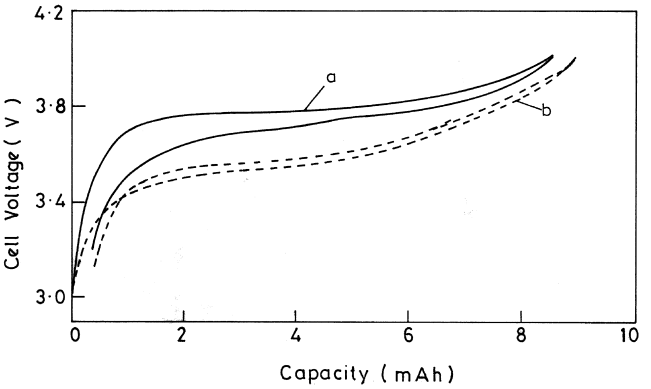

Fig. 10. Curves depicting hysteresis in the charge–discharge profiles of (a) $LiCoO_2$ and (b) $LiNi_{0.4}Co_{0.6}O_2$.

All the cathode materials were cycled against lithium between 4.2 and 3.0 V in cathode-limited coin cells. The charge and discharge capacities at the 1st and 25th cycles for cells with the five respective cathode compositions are shown in Fig. 11. A gradual increase in the cell capacity may be noted with increase in the nickel content. The values for $Li/Li_xNi_yCo_{1-y}O_2$ cells with $y=0$ are 146 mAh and 132 mAh in the first cycle, and 126 mAh and 118 mAh in the 25th cycle which translates to a loss of 0.56 mAh per cycle. The respective values for the cell with $LiNi_{0.4}Co_{0.6}O_2$ are 160 mAh and 148 mAh for the 1st cycle, and 134 mAh and 125 mAh for the 25th cycle representing a loss of 0.92 mAh per cycle. Intermediate values were recorded for the other compositions. Discharge capacities for all the compositions as a function of cycle number are plotted in Fig. 12. Further cycling studies are in progress.

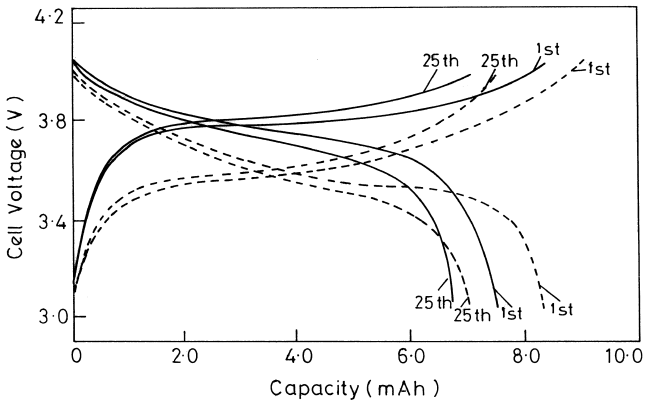

Fig. 9. Charge–discharge profiles of $LiCoO_2$ (solid lines) and $LiNi_{0.4}Co_{0.6}O_2$ in the 1st and 25th cycles. Rate: 50 μA.

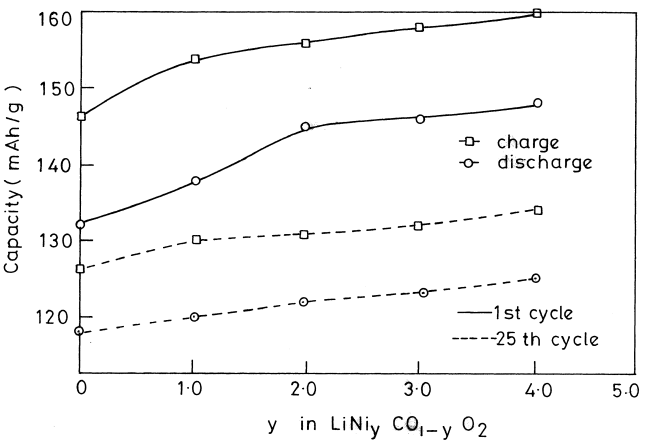

Fig. 11. First charge and discharge capacities at the 1st and 25th cycles for cells with the five respective cathode compositions.

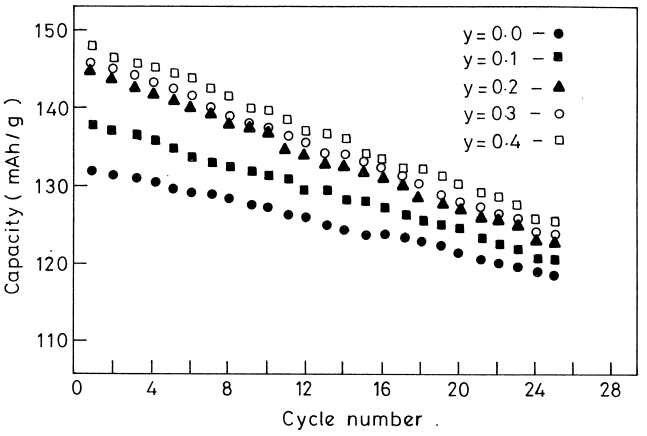

Fig. 12. Discharge capacities for the various compositions as a function of cycle number.

4. Conclusions

$LiCoO_2$ and nickel substituted $LiCoO_2$ have been synthesized using solid state fusion method. XRD studies, complemented by FTIR data, show little or no evidence of cation mixing disorder in the compounds. A knee region on the discharge curves of the nickel substituted compounds show that the oxidation of Ni^{3+} precedes that of Co^{3+}. Nickel substituted $LiCoO_2$ compounds show not only higher discharge capacities but also smaller hystereses in the charge–discharge profiles. Thus they appear to be attractive candidates for use as cathodes in lithium-ion cells. However, despite its lower discharge capacity, $LiCoO_2$ exhibits reduced fades upon cycling which qualifies it for long cycle-life cells.

References

[1] Ohzuku T, Komori H, Sawai K, Hirai T. Chem Exp 1990;5:733.
[2] Delmas C, Saadoune I. Solid State Ionics 1992;53–56:370.
[3] Delmas C, Saadoune I, Rougier A. J Power Sources 1993;43–44:595.
[4] Ohzuku T, Ueda U, Nagayama M, Iwakoshi Y, Komori H. Electrochim Acta 1993;38:1159.
[5] Mizushima K, Jones PC, Wiseman PJ, Goodenough JB. Mater Res Bull 1980;15:783.
[6] Dahn JR, von Sacken U, Michal CA. Solid State Ionics 1990;44:87.
[7] Zhecheva E, Stoyanova R. Solid State Ionics 1993;66:143.
[8] Rougier A, Saadoune I, Gravereau P, Willmann P, Delmas C. Solid State Ionics 1996;90:63.
[9] Saadoune I, Delmas C. J Mater Chem 1996;6:193.
[10] Dyer LD, Borie BS, Smith GP. J Am Chem Soc 1954;76:1499.
[11] Morales J, Perez-Vicente C, Tirado JL. Mater Res Bull 1990;25:623.
[12] Fujita Y, Amine K, Maruta J, Yasuda H. J Power Sources 1997;68:126.
[13] Choi YM, Pyun SI, Moon SI, Hyung SE. J Power Sources 1998;72:83.
[14] Gummow RJ, Thackeray MM. Solid State Ionics 1992;53–56:681.
[15] Choi YM, Pyun SI, Moon SI. Solid State Ionics 1996;89:43.
[16] Julien C, Michael SS, Ziolkiewicz S. Int J Inorg Mater 1999;1:29.
[17] Rougier A, Nazri GA, Julien C. Ionics 1997;3:170.
[18] Nazri M, Curtis D, Yebka B, Nazri GA, Julien C. In: Ext. Abstract 193rd Meeting of the Electrochemical Society, 1998.
[19] Lundbald A, Bergman B. Solid State Ionics 1997;96:173.
[20] Ahmed AI, El-Hakam SA, Samra SE. Ind J Chem Sec A 1990;29:470.
[21] Lide DR. Handbook of Chemistry and Physics, 74th ed., The Chemical Rubber, Ohio. 1993-94.
[22] Malik WU, Gupta DR, Masood I, Gupta RS. J Mat Sci Lett 1985;4:532.
[23] Reisman A. J Am Chem Soc 1958;80:3558.
[24] Smirnov MV, Lyubimtseva I, Tsiovkina LA, Krasnov YN. Russ J Inorg Chem 1971;16:130.
[25] Snell FD, Ettre LS, editors, Encyclopaedia of Industrial Chemical Analysis, vol. 16, New York: Interscience Publishers, 1972, p. 342.
[26] Barboux P, Tarascon JM, Shokoohi FK. J Solid State Chem 1991;94:185.
[27] Gummow RJ, Thackeray MM, David WIF, Hull S. Mater Res Bull 1992;27:327.
[28] Gummow RJ, Thackeray MM. Soild State Ionics 1992;53–56:681.
[29] Lagergren C, Lundblad A, Bergman B. J Electrochem Soc 1994;141:2959.
[30] Garcia B, Barboux P, Ribot F, Kahn-Harari A, Mazerolles L, Baffier N. Solid State Ionics 1995;80:111.
[31] Cuarant D, Baffier N, Garcia B, Pereira-Ramos JP. Soild State Ionics 1996;91:45.
[32] Alcantara R, Morales J, Tirado JL, Stoyanova R, Zhecheva E. J Electrochem Soc 1995;142:3997.